IEEE Photonics Journal
An IEEE Photonics Society Publication

Technology Requirements for an Alamouti-Coded 100 Gb/s Digital Coherent Receiver Using 3 × 3 Couplers for Passive Optical Networks

Volume 10, Number 1, February 2018

Md. Saifuddin Faruk, *Member, IEEE*
David J. Ives
Seb J. Savory, *Fellow, IEEE*

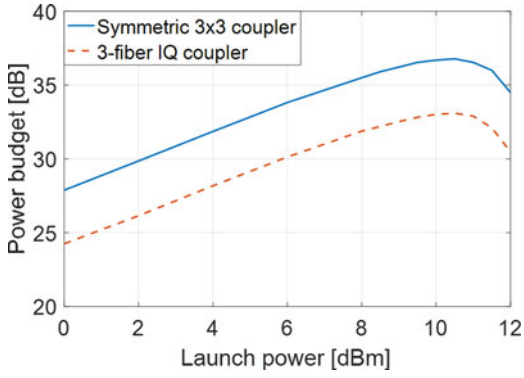

DOI: 10.1109/JPHOT.2017.2788191
1943-0655 © 2017 CCBY

Technology Requirements for an Alamouti-Coded 100 Gb/s Digital Coherent Receiver Using 3 × 3 Couplers for Passive Optical Networks

Md. Saifuddin Faruk,[1] ***Member, IEEE***, **David J. Ives**,[2] **and Seb J. Savory**,[2] ***Fellow, IEEE***

[1]Department of Electrical and Electronic Engineering, Dhaka University of Engineering and Technology, Gazipur 1700, Bangladesh
[2]Engineering Department, Electrical Engineering Division, University of Cambridge, Cambridge CB3 0FA, U.K.

DOI:10.1109/JPHOT.2017.2788191

Manuscript received December 18, 2017; accepted December 26, 2017. Date of publication January 8, 2018; date of current version January 22, 2018. This work was supported in part by the EU project ICONE (608099) and in part by EPSRC through INSIGHT (EP/L026155/2) and UNLOC (EP/J017582/1).
Corresponding author: Md. Saifuddin Faruk (e-mail: faruk@duet.ac.bd).

Abstract: Digital coherent receivers employing Alamouti-coding are a promising solution for passive optical networks (PON) with downstream rates of 100 Gb/s/λ. To reduce the cost by utilizing high-volume photodiodes designed for 25 Gb/s data-center applications, we consider 28-Gbaud 16-QAM modulation format detected with a single-polarization coherent receiver based on a 3 × 3 coupler with single-ended detection. We investigate two alternative configurations: first, a receiver with a symmetric 3 × 3 coupler and second, an IQ coupler (asymmetric 3 × 3 coupler) with Alamouti-coding based polarization diversity. In this paper, we present a detailed investigation as to the feasibility of both the receivers for a wide range of parameters including quantization noise, relative intensity noise, I/Q mismatch, etc. It is found that such receivers can be realized with commercially available components. We also quantify the penalty associated with nonideal components to allow for lower cost designs with reduced specifications suitable for access applications. In addition, we present the adaptive DSP algorithms required to recover data for a single-carrier Alamouti-coded signal. Considering both linear and nonlinear impairments, a power budget of 36.4 dB and 33.1 dB is found at BER of 3.8×10^{-3} for a receiver with symmetric 3 × 3 coupler and IQ coupler, respectively, and thereby proving their applicability as receivers for 100 Gb/s/λ PON.

Index Terms: Passive optical networks (PON), coherent detection, digital signal processing.

1. Introduction

The data rate supported by a passive optical network (PON) needs to keep pace with the ever increasing demands of users. The next development for PON is 100 Gb/s per fiber with the IEEE P802.3ca 100G-EPON Task Force already discussing standardization, targeting 25/50/100 Gb/s PON based on a 25 Gb/s per wavelength line-rate [1], [2]. While the multi-wavelength solution allows 25 Gb/s components developed for data centers to be utilized, an alternative approach is to target a 25 GBd single wavelength solution to achieve 50 Gb/s [3] or 100 Gb/s [4].

Transmission of single wavelength 100 Gb/s has already been deployed in core networks; for example, using 28-Gbaud dual-polarization quadrature phase shift keying (DP-QPSK) signal was demodulated by digital coherent receivers [5]. The receiver used for such purpose are usually employed with a phase and polarization diversity configuration consisting of optical 90° hybrids, polarization beam splitters (PBS), balanced photo-diodes, transimpedance amplifier (TIA), analog-to-digital converter (ADC) and digital signal processing (DSP) based demodulator [6]. However, due to stringent requirement of cost, such receiver is not suitable as a receiver in optical network unit (ONU) of an access network. Therefore, simplification of coherent receivers is required to introduce them in the PON application.

One of the common ways to reduce the receiver complexity is to use a single-polarization receiver which requires half of the components compare to conventional polarization-diversity receiver. However, the key problem of such receiver is that the receiver sensitivity is dependent on the state of polarization (SOP) of the incoming signal. In the worst case, where the SOP of the incoming signal is orthogonal to that of the local oscillator (LO), the receiver cannot detect the transmitted signal [7]. In practical systems, the polarization of the incoming signal is unlikely to remain aligned to the SOP of the LO because of random changes on the birefringence of the transmission fiber and thus measure needs to be taken to make it polarization independent. Polarization insensitivity can be achieved either at receiver side, for example, using additional PBS [8] or at transmitter side, for example, using Alamouti space-time block coding (STBC) [9], two-lasers with orthogonal polarization states [10], DGD-predistortion technique [11] etc. For PON application, transmitter-side diversity is preferable since equipments at optical line terminal (OLT) are shared by all users and thus system cost is reduced.

A simple receiver with a 3×3 coupler and no-DSP has been demonstrated for PON applications in [8], [12]. However, such receiver can be operated for only OOK modulation format and not suitable to support beyond 10 Gb/s. Moreover, for polarization diversity a PBS is used in the receiver whose monolithic integration is challenging. Recently, we have demonstrated a simple phase diversity coherent receiver based on Alamouti STBC polarization coding and heterodyne detection for 10 Gb/s PON application [9], [13]. Such receiver is comprised of only single balanced photo-diode, one TIA and an ADC. However, it is difficult to realize high data rate system with heterodyne detection due to higher bandwidth requirement of receiver components that results higher cost. Keeping this in mind and targeting to use 25 Gb/s components developed for mass-volume data center applications, in this work, we propose 28-Gbaud 16-quadrature amplitude modulation (16-QAM) format to realize 100 Gb/s[1] PON which is detected by a simple single-polarization homodyne coherent receiver with transmitter-side polarization diversity based on Alamouti STBC. Unlike commonly used coherent receiver employing 90° hybrids followed by balanced photodiodes, in this work, we consider 3×3 coupler based receiver that allows using cheaper single-ended photodiodes. Two receiver configurations are investigated: using a symmetric 3×3 coupler with three single-ended photodiodes and a much simpler configuration (however, allowing a modest sensitivity degradation) with a 3-fiber IQ coupler with two single-ended photodiodes. Performance of the proposed transceivers are analyzed in detailed with intensive computer simulation.

Albeit receiver with 3×3 couplers and Alamouti STBC based polarization diversity scheme are separately available in literatures, herein presents several new key contributions. Firstly, applicability of the simplified single-polarization phase diversity coherent receiver with a symmetric 3×3 coupler and with a 3-fiber IQ coupler for 100 Gb/s PON system is verified for the first time. Considering both linear and nonlinear impairments, it is shown that the power budgets achieved with such receivers exceed the typical values available for current 10 Gb/s PON solutions. Secondly, performance of both receivers are investigated over a range of system parameters such as LO relative intensity noise (LO-RIN), ADC quantization noise, coupler imperfection, fiber nonlinearity and so on. Thirdly, a comparative analysis of performance and implementation complexity is presented for both of the receivers. Particularly to mention, the impact of coupler imperfection and its DSP-based mitigation

[1]Since Alamouti STBC is a half-rate coding [14], 28-Gbaud 16-QAM signal will results an aggregate data rate of 112 Gb/s even a DP transmitter is used.

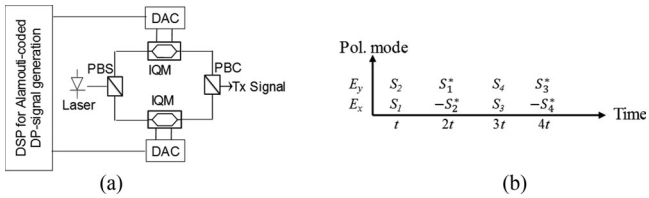

Fig. 1. A DP transmitter employing Alamouti STBC in two polarization tributaries. (a): transmitter configuration, (b): illustration of Alamouti STBC in two polarization modes.

method for them are quite different and obscure which are rigorously investigated and explained. Finally, an improved DSP technique for equalization, polarization tracking and carrier phase estimation based on least-mean-square (LMS) algorithm is presented for single-carrier (SC) Alamouti coded signal. Unlike [13], we include a single-input single-output adaptive filter prior to polarization tracking which performs ADC sampling phase adjustment, matched filtering and equalization of chromatic dispersion all at once. Since the configuration of the DSP scheme is different compare to that used in a conventional SC dual-polarization receiver, we present the explicit derivation of the adaptation algorithms.

The rest of the paper is organized as follows: Section 2 describes the configuration and principle of proposed transceiver and related DSP algorithms for 100G-PON. Simulation results for 40-km transmission of 28-Gbaud 16-QAM signal employing the proposed transceiver is demonstrated in Section 3 and finally we conclude the paper in Section 4.

2. Proposed Transceivers for 100G PON

2.1 Transmitter Configuration

To enable transmitter-side polarization diversity, a DP transmitter as shown in Fig. 1(a) is used employing 28-Gbaud 16-QAM signal. However, in contrast to conventional DP transmitter where two independent data symbols are sent on $x-$ and $y-$ polarization modes, Alamouti coded signals are used in two polarization channels.

For Alamouti STBC, the symbols are grouped into pairs of time slots. In the first symbol period the symbols S_1 and S_2 are sent whereas in the next symbol period $-S_2^*$ and S_1^* are sent on $x-$ and $y-$ polarization modes, respectively; where $(\cdot)^*$ denotes the complex conjugate operation. The coding sequence is illustrated in Fig. 1(b). Therefore, in two orthogonal polarization modes ($[E_x\ E_y]$), two symbol-pairs $[S_1\ S_2]$ and $[-S_2^*\ S_1^*]$ are transmitted which are orthogonal and ensure that for any state of polarization of the channel, no information is lost even a single polarization is detected. Appropriate DSP operations in the receiver then allows tracking of channel polarization states and subsequently demodulation of the data.

2.2 Receiver With Symmetric 3 × 3 Coupler

The architecture of single-polarization phase-diversity homedyne coherent receiver using a symmetric 3 × 3 coupler is shown in Fig. 2(a). Optical signals from the three output ports of the coupler are detected by three photodiodes followed by TIAs and ADCs. The operations to obtain I and Q components of the signal from three photo-detected currents are obtained in the digital domain.

The scattering matrix for 3 × 3 fiber coupler is given by [15]:

$$\mathbf{S} = \begin{pmatrix} a & b & b \\ b & a & b \\ b & b & a \end{pmatrix} \tag{1}$$

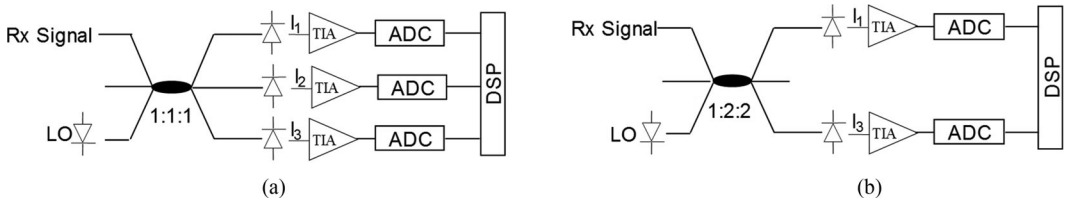

Fig. 2. Phase diversity homodyne receiver employing (a): a 3 × 3 symmetric coupler and (b): a 3-fiber IQ coupler.

where a and b are related to coupling coefficient κ and interaction length l as follows:

$$a = \frac{2}{3}e^{j\kappa l} + \frac{1}{3}e^{-j2\kappa l}$$
$$b = \frac{1}{3}e^{-j2\kappa l} - \frac{1}{3}e^{j\kappa l}. \tag{2}$$

For $\kappa l = \frac{2\pi}{9}$ the coupler has a symmetric power coupling ratio of 1:1:1 [16]. As shown in Fig. 2(a), if the two ports of such coupler has incoming optical signal field E_s and LO field E_L, three output currents after photo-detection are given by:

$$I_1 = |a|^2|E_s|^2 + |b|^2|E_L|^2 + 2\,\mathrm{Re}\,(ab^*E_L^*E_s)$$
$$I_2 = |b|^2|E_s|^2 + |b|^2|E_L|^2 + 2\,\mathrm{Re}\,(|b|^2E_L^*E_s)$$
$$I_3 = |b|^2|E_s|^2 + |a|^2|E_L|^2 + 2\,\mathrm{Re}\,(a^*bE_L^*E_s)\,. \tag{3}$$

From three detected currents shown in (3), we can easily obtain the I and Q components of the signal using the simple operations as below:

$$I_I = I_2 - 0.5(I_1 + I_3)$$
$$I_Q = \sqrt{3}/2(I_3 - I_1) \tag{4}$$

Performing the operation of (4) ensures that the DC terms are automatically eliminated as in a conventional balanced receiver [17]. This also assures the cancellation of direct-detection signal term and LO-RIN impact on the system performance. This balancing operation can be done using analog circuits before ADCs or can be performed digitally after ADCs. In this work, we choose the later option since it provides the flexibility to correct the imperfections of receiver components in the digital domain.

2.3 Receiver With 3-Fiber IQ Coupler

Using a 3-fiber IQ coupler simplifies the receiver by dropping one photo-diode, TIA and ADC compare to the configuration shown in Fig. 2(a).The IQ coupler can be made by setting $\kappa l = \frac{2}{3}\left(m\pi \pm \tan^{-1}3\right)$ in making a 3 × 3 fiber coupler which provides an output power coupling ratio of 1:2:2 with an phase angle of 90° between coherent term of port 1 and 3, where m is an integer. In such a case, the 3 × 3 coupler works as an IQ coupler. Since $\tan^{-1}3 < \pi/2$, the minimum coupling length is $\kappa l = \frac{2}{3}\left(\tan^{-1}3\right)$, for which the scattering matrix is given as [18]:

$$\mathbf{S}_{IQ} = \begin{pmatrix} \sqrt{\frac{1}{5}} & \sqrt{\frac{2}{5}}e^{j\frac{3\pi}{4}} & \sqrt{\frac{2}{5}}e^{j\frac{3\pi}{4}} \\ \sqrt{\frac{2}{5}}e^{j\frac{3\pi}{4}} & \sqrt{\frac{1}{5}} & \sqrt{\frac{2}{5}}e^{j\frac{3\pi}{4}} \\ \sqrt{\frac{2}{5}}e^{j\frac{3\pi}{4}} & \sqrt{\frac{2}{5}}e^{j\frac{3\pi}{4}} & \sqrt{\frac{1}{5}} \end{pmatrix} \tag{5}$$

where, the elements of (5) are normalized such that the leading diagonal terms are real.

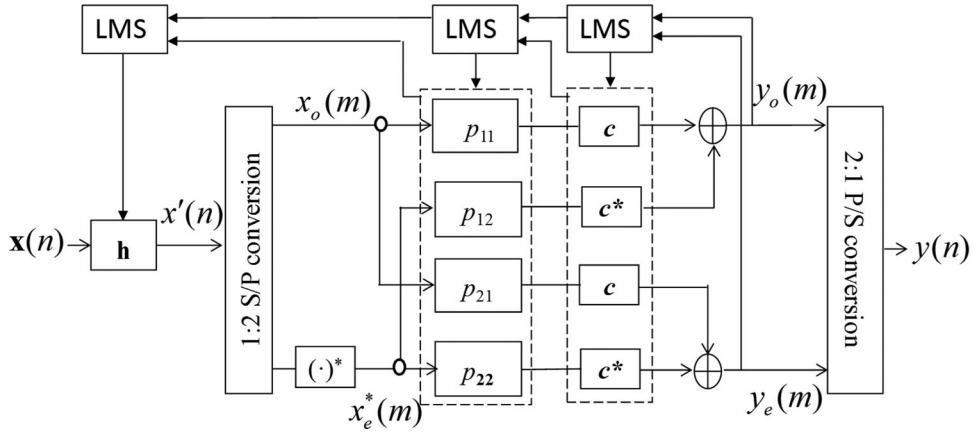

Fig. 3. DSP operations to demodulate SC Alamouti STBC signal.

In this case, the photo-currents from port 1 and 3 can be expressed as [19]:

$$I_1 = \frac{1}{5}|E_s|^2 + \frac{2}{5}|E_L|^2 + \frac{2\sqrt{2}}{5}\,\mathrm{Re}\,(E_L^* E_s)$$
$$I_3 = \frac{2}{5}|E_s|^2 + \frac{1}{5}|E_L|^2 - \frac{2\sqrt{2}}{5}\,\mathrm{Im}\,(E_L^* E_s)\,. \tag{6}$$

As shown in (6), the I and Q term of the signal can be found from coherent term of I_1 and I_3, respectively. Typically, $|E_L|^2 \gg |E_s|^2$ and thus the direct-detection term is dominated by $|E_L|^2$ which is nearly constant. By blocking the DC term of detected I_1 and I_3 (in this work which is done in DSP), we constitute the received complex signal which is processed with the DSP describe in Section 2.4 to recover the information. Albeit the receiver front-end is simpler compare to that of Fig. 2(a), it comes with an expense of sensitivity degradation since the signal in the output port-2 of the coupler remains unused [20] as well as the impact LO-RIN cannot be neglected any more. Note that to enable common-mode noise rejection,we have to use all three output ports of such asymmetric coupler [19]; however, in this work, we consider the configuration shown in Fig. 2(b) for its low-complexity implementation by allowing modest sensitivity degradation. The performance of such receiver are discussed in detail in Section 3.4.

2.4 DSP for Recovering SC Alamouti STBC Signal

To demodulate the data for SC Alamouti STBC signal received by a single polarization receiver, the received signal is processed with the DSP similar to [13] with an additional adaptive equalizer as shown in Fig. 3. The multi-tap single-input single-out FIR filter **h** performs the functionalities of CD compensation, matched filtering and ADC sampling-phase adjustment, the single-tap variable p tracks the polarization states and another single-tap variable c carries out carrier phase estimation. For adaptation of **h**, p and c, the LMS algorithm is used.

As shown in Fig. 3, the even and odd indexed output can be written as:

$$y_o(m) = x_o p_{11} c + x_e^* p_{12} c^*$$
$$y_e(m) = x_o p_{21} c + x_e^* p_{22} c^* \tag{7}$$

where, $x_o = \mathbf{h}^T \mathbf{x}(n-1)$ and $x_e = \mathbf{h}^T \mathbf{x}(n)$. The superscript $(\cdot)^T$ denotes the transpose operation. For a N-tap filter, we define the tap-coefficient vector $\mathbf{h} = [h_0, h_1, \cdots, h_{N-1}]^T$ and filter input vector $\mathbf{x}(n) = [x(n), x(n-1), \cdots, x(n-(N-1))]^T$. Also, n is the symbol-spaced sample index and m is the two-symbols-spaced sample index.

Using the LMS algorithm, the error signals for the phase estimator can be written as:

$$e_o = d_o - y_o$$
$$e_e = d_e - y_e \tag{8}$$

where, $d_{o,e}$ is the training symbol at the start-up that ensure fast and reliable convergence and decided symbol from $y_{o,e}$ in the steady-state decision-directed (DD) mode. The value of c is updated using a convergence parameter of μ_c as (detail derivation is shown in the appendix):

$$c \leftarrow c + \mu_c \left[e_o x_o^* p_{11}^* + e_o^* x_e^* p_{12} + e_e x_o^* p_{21}^* + e_e^* x_e^* p_{22} \right] \tag{9}$$

Estimated phase is then used to find the error signals for polarization tracker as [21]:

$$e_{11} = d_o \{c/|c|\}^{-1} - x_o p_{11}$$
$$e_{12} = d_o \left\{c^*/|c|\right\}^{-1} - x_e^* p_{12}$$
$$e_{21} = d_e \{c/|c|\}^{-1} - x_o p_{21}$$
$$e_{22} = d_e \left\{c^*/|c|\right\}^{-1} - x_e^* p_{22} \tag{10}$$

and correspondingly the update equations are given as:

$$p_{11} \leftarrow p_{11} + \mu_p e_{11} x_o^*$$
$$p_{12} \leftarrow p_{12} + \mu_p e_{12} x_e$$
$$p_{21} \leftarrow p_{21} + \mu_p e_{21} x_o^*$$
$$p_{22} \leftarrow p_{22} + \mu_p e_{22} x_e \tag{11}$$

Finally, $\mathbf{h}$ is updated in every two-symbols as below (detail derivation is shown in appendix):

$$\mathbf{h} \leftarrow \mathbf{h} + \mu_h \left\{ e_{11} \mathbf{x}^*(n-1) p_{11}^* + e_{12}^* \mathbf{x}^*(n) p_{12} + e_{21} \mathbf{x}^*(n-1) p_{21}^* + e_{22}^* \mathbf{x}^*(n) p_{22} \right\} \tag{12}$$

3. Simulation Investigations

3.1 Simulation Setup

To evaluate the performance of the proposed transceiver, we conduct computer simulation for 28-Gbaud 16-QAM transmission systems using the proposed transceivers. The SC Alamouti coded signal is generated by a DP transmitter configured as in Fig. 1(a). A pulse shaping filter having a root-raise cosine (RRC) profile with a roll-off factor of 0.1 is employed. The signal is then transmitted over 40-km standard single mode fiber (SMF) having dispersion coefficient, $D = 16$ ps/nm/km, attenuation coefficient, $\alpha_{dB} = 0.25$ dB/km and nonlinearity coefficient, $\gamma = 1.3$ W/km. The signal is then detected with the receiver shown in Fig. 2(a) or (b). A variable optical attenuator (VOA) is used before the receiver to control the incoming signal power. The receiver noise considered are shot noise, thermal noise and RIN from LO, which are the dominant sources of noise in an unamplified transmission system [22]. To simulate the overall bandwidth of the receiver, we use a 3rd-order Bessel low pass filter with the 3-dB cutoff frequency denoting receiver bandwidth. Unless stated the following parameters are considered in the simulation: LO power = 7 dBm, LO-RIN = −150 dB/Hz, LO 3-dB linewidth = 1 MHz, thermal noise current density of TIA = 18.2 pA/$\sqrt{Hz}$, resolution of ADC = 6 bits, and receiver bandwidth = 18 GHz.

The received electrical signal is digitized by the ADCs at a rate of twice the symbol rate. First, the received complex-valued samples are formed by calculating I and Q components using (4) for receiver with symmetric coupler or directly from the coherent terms of signal from port-1 and port-3 for IQ coupler. Then, the following identical DSP operations are performed for both the receiver configurations: frequency offset compensation based on observing the peak in the spectrum of 4-th power of signal [23] and adaptive equalization, polarization tracking and carrier phase recovery using the DSP described in Section 2.4. The number of taps for filter h is 17 which found enough

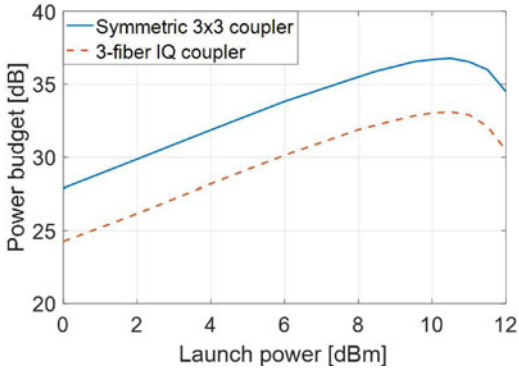

Fig. 4. Power budget as a function of launch power.

to perform the compensation of CD stemmed form 40-km SMF and also to perform RRC matched filtering for 0.1 roll-off factor [24]. We use the optimized step-size parameters that gives the lowest BER. A total of 2×10^5 symbols are processed from which first 60×10^3 symbols are used for training. Finally, the symbols are differentially decoded and the bit-error-rate (BER) is measured by direct counting method.

3.2 Optimum Launch Power

To maximize performance of an access network the optimal launch power needs to be determined, since this then allows all subsequent simulations to be performed including both linear and nonlinear impairments. To determine the optimum launch power we measure the power budget[2] as a function of launch power for 40-km unrepeated transmission over standard SMF as shown in Fig. 4. The optimum launch power is found 10.5 dBm for both receiver configuration which is used to obtain the rest of the results.The receiver sensitivity is found lower in asymmetric coupler based receiver compare to symmetric one. Such degradation is mainly due to use of lesser LO power for not utilizing output port-2 [20].

The power budget for receiver with symmetric 3×3 coupler is found as 36.4 dB that enable 1:128 way split after 40-km of transmission with 1.9 dB margin[3]. On the other hand, for the receiver 3-fiber IQ coupler, the power budget is found 33.1 dB which can also support 1:64 way split and 40-km of transmission with a margin of 2.1 dB.

3.3 Performance of the Symmetric 3×3 Coupler Based Receiver

Now, we consider the receiver shown in Fig. 2(a) and investigate the impact of ADC bit resolution and RIN. The BER against received power for different ADC bit resolution is illustrated in Fig. 5(a). The ADC resolution of 6-bits seems to be sufficient. The receiver sensitivity is found -25.9 dBm at BER of 3.8×10^{-3} (7% FEC limit). Fig. 5(b) shows the impact of LO-RIN on the BER performance. As expected, the system performance is found independent of LO-RIN even with a large value of -140 dB/Hz. This is due to balancing operation done in (4).

Next, we investigate the tolerance of LO phase noise and frequency offset as shown in Fig. 6. Fig. 6(a) shows the required receiver sensitivity at 7% FEC limit as a function of 3-dB linewidth of LO. It is found that, linewidth tolerance is 3 MHz for 1-dB sensitivity penalty and more than 5 MHz for 2-dB penalty. Therefore, a conventional distributed feedback (DFB) laser can be used as LO. To investigate the tolerance of frequency offset, we measure the BER for different frequency offset values at a received power of -25 dBm which is shown in Fig. 6(b). The frequency offset tolerance largely depends on receiver bandwidth. For a receiver bandwidth of 18 GHz, no significant BER degradation

[2]Power budget is the difference between launch power and receiver sensitivity at BER of 3.8×10^{-3}.
[3]The link loss is considered as power loss in fiber at 0.25 dB/km and splitter loss at 3.5 dB/ two-way split.

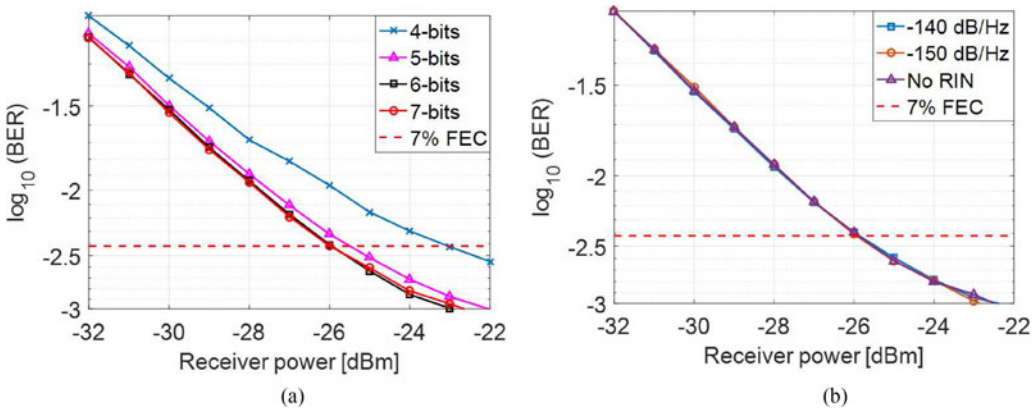

Fig. 5. The BER performance of receiver with symmetric 3×3 coupler as a function of received power (a): for different ADC resolutions (b): for different LO-RIN values.

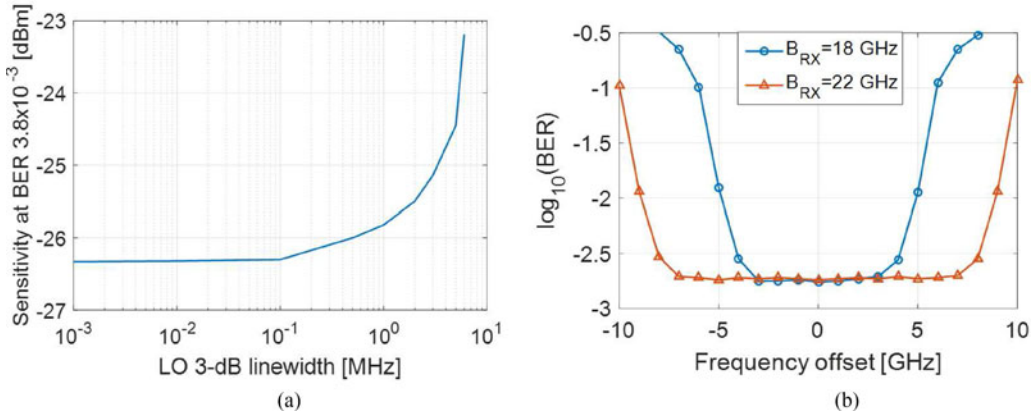

Fig. 6. Tolerances of LO phase noise frequency offset for 28-Gbaud 16-QAM signals.(a): required sensitivity at BER of 3.8×10^{-3} as a function of 3-dB linewidth of LO, (b): the BER performance for different frequency offset at a received power of -25 dBm.

is observed for the frequency offset about ± 4 GHz. This range is increased to ± 8 GHz for a receiver bandwidth of 22 GHz suggesting that increasing the receiver bandwidth enhances the tolerance accordingly.

We also investigate the impact of small manufacturing imperfection of fused 3×3 coupler where the imbalance stem from small maladjustment of interaction length. The imperfection of the coupler is emulated by changing the value of κl with a parameter α defined as $\kappa l = \frac{2\pi}{9}[1 \pm \alpha]$. As shown in Fig. 7(a), at $\alpha = 0$, the power in three output ports of the coupler are same while the phase angle difference is 120° between port-3 and port-1 or port-2. Slightly over pulling ($\alpha > 0$) in making the coupler causes more power coupled in port-1 and port-2 with an phase angle difference greater than 120° from port-3. The opposite happens for under pulling case ($\alpha < 0$). However, it is important to note that, after the IQ conversion operation given by (4), the phase angle difference between I and Q signals always remains 90°. This property allows us correcting the imperfection in the DSP by simply setting the mean square values of three currents equal before further signal processing (no orthogonalization is required). The performance of such DSP operation is illustrated in Fig. 7(b), where the BER is plotted against α parameter for a received power of -25 dBm. It is found that BER performance can be seriously degraded if no mitigation technique is used; however, with mitigation in the DSP, the performance improves significantly and the BER is always found below the FEC limit over the observed $\pm 15\%$ imbalance of κl.

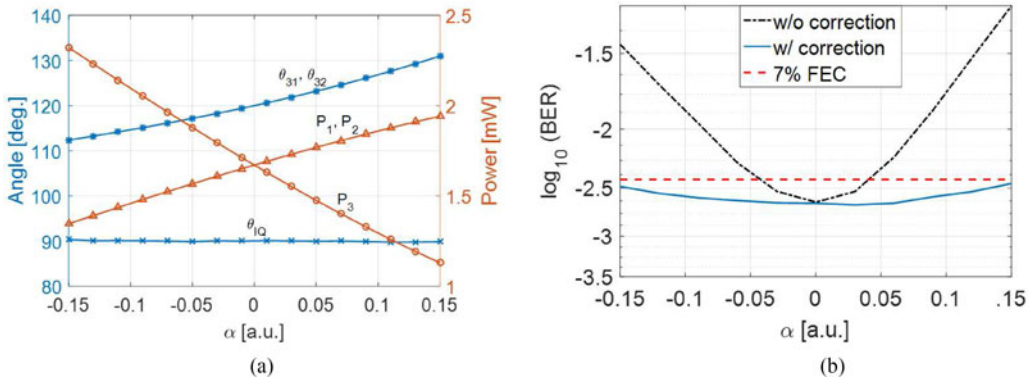

Fig. 7. Impact of coupling imperfection of symmetric 3 × 3 coupler- (a): changes of angle and power in the output ports due to imperfection, and (b): the BER performance with and without DSP correction.

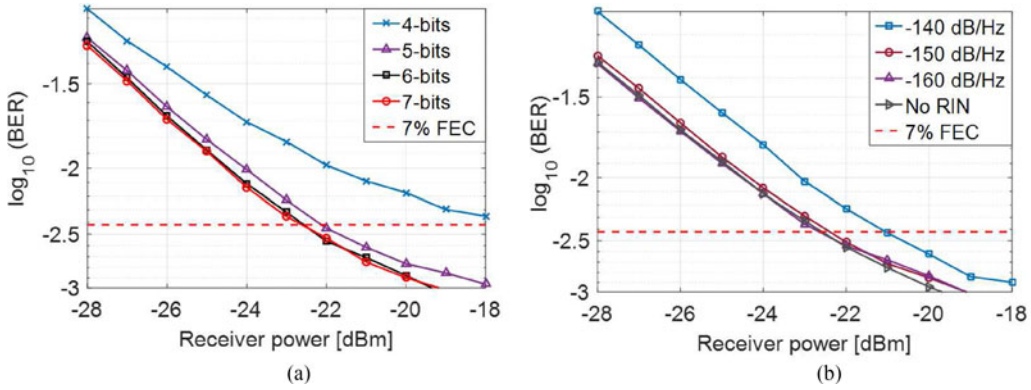

Fig. 8. The BER performance of receiver with 3-fiber IQ coupler as a function of received power (a): for different ADC resolutions (b): for different LO-RIN values.

3.4 Performance of the 3-Fiber IQ Coupler Based Receiver

The BER performance as a function of received power using the receiver with 3-fiber IQ coupler is shown in Fig. 8. The impact of ADC bit resolution is depicted in Fig. 8(a). Similar to receiver with symmetric coupler, it is found that an ADC resolution of at least 6-bits is required to avoid any significant performance degradation. The receiver sensitivity at BER of 3.8×10^{-3} is found as -22.6 dBm which is 3.3 dBm less than receiver with symmetric coupler. This is mainly due to the fact that the power from output port-2 (40% of the total power) of coupler remains used. The impact of LO-RIN is shown in Fig. 8(b). Unlike the receiver with symmetric coupler, the performance is no longer LO-RIN independent, since no common mode noise rejection operation is involved. However, no significant penalty is observed for LO with less than -150 dB/Hz RIN.

The LO phase noise and frequency offset tolerances are observed similar to those for receiver with symmetric coupler. This is because such tolerances depend on the algorithm used for those impairment estimation rather than receiver configuration.

Next, we investigate the impact of coupler imperfection. In this case, the α parameter is defined as $\kappa l = \frac{2}{3}\tan^{-1} 3[1 \pm \alpha]$. For $\alpha = 0$ the phase angle between coherent terms of I_1 and I_3 (i.e., I and Q signals) is 90°. However, this angle increases for $\alpha < 0$ and decreases for $\alpha > 0$ causing IQ imbalance as shown in Fig. 9(a). However, such IQ imbalance can be corrected in the DSP, for example, using the Gram-Schmidt orthogonalization procedure (GSOP) [25]. The BER performance with and without GSOP is shown for a received power of -21 dBm in Fig. 9(b). It is found that without GSOP the BER drastically increase with increasing α value. A significant performance

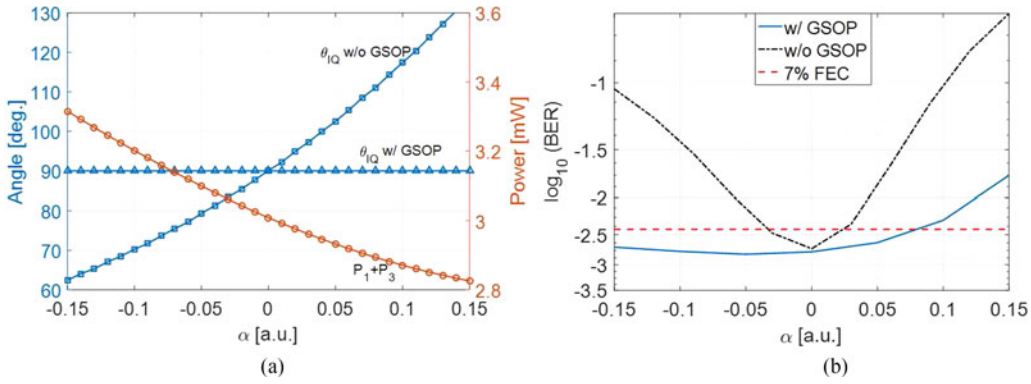

Fig. 9. Impact of coupling imperfection of 3-fiber IQ coupler- (a): changes of angle between *I* and *Q* ports and total received power by port-1 and port-3 due to imperfection, and (b): the BER performance with and without GSOP.

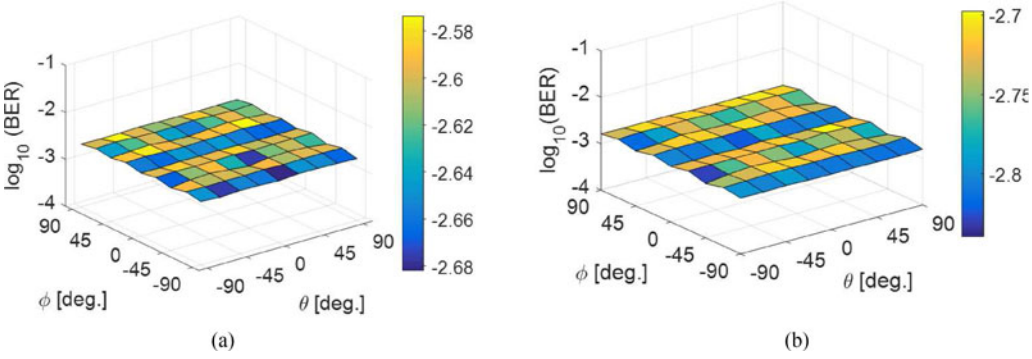

Fig. 10. The BER performance for two-dimensional sweep of polarization states. (a): for receiver with symmetric 3 $\times$ 3 coupler and (b): receiver with 3-fiber IQ coupler.

improvement can be achieved by applying GSOP; however, the improvement is asymmetric for over pulled and under pulled conditions. As shown in Fig. 9(a), with an increasing α values, the IQ phase imbalance increases as well as total coupled power in port 1 and 3 decreases. Both the phenomena tend to increase the BER, nevertheless, applying the GSOP improves the performance compare to no correction condition. On the other hand, with deceasing α value, albeit the IQ phase imbalances increases, the total power coupled to port 1 and 3 also increases which tends to improve the BER performance. Thus, when we apply the GSOP to correct the IQ imbalance, the BER performance is slightly improved even compare to the ideal case of $\alpha = 0$. The best performance is observed at 5% under pulling condition. Thus, it can be suggested that in making the coupler, slightly under pulled condition should be considered rather than the ideal case to obtain the optimum performance.

3.5 Verification of Polarization-Insensitive Operation

We verify the polarization insensitive operation of the proposed single-polarization receivers which is enabled by Alamouti STBC at the transmitter. The SOP of the incoming signal to receiver is emulated using the Jones matrix:

$$\mathbf{J} = \begin{bmatrix} \cos\theta & \sin\theta e^{-j\phi} \\ -\sin\theta\, e^{j\phi} & \cos\theta \end{bmatrix} \tag{13}$$

where, 2θ and ϕ are the azimuth and elevation rotation angles between two polarization states, respectively. To evaluate the tolerance of polarization changes over the entire Poincaré sphere, the parameters θ and ϕ in (13) are swept between $-\pi/2$ to $+\pi/2$. Fig. 10 shows the BER performance for such two-dimensional sweep. The received power are -25 dBm and -21 dBm for the receiver with symmetric coupler and 3-fiber IQ coupler, respectively. No significant performance variation is observed for any polarization rotation confirming the polarization-insensitive operation of the proposed receivers.

4. Conclusion

We have demonstrated simple single-polarization coherent receivers using a 3×3 coupler and single-ended detection, aiming at the application of 100 Gb/s/λ PON. Polarization insensitivity is achieved using Alamouti STBC at the transmitter. Two receiver configurations are investigated: receiver with a symmetric 3×3 coupler and a 3-fiber IQ coupler. The former shows better performance while the later one has less complexity. As to the technology requirements, with rigorous investigation we confirm that such receivers for 100G PON application can be realized with current commercially available components including distributed-feedback (DFB) laser, photodiode and ADC. The performance of the transceiver has been demonstrated with intensive computer simulation of 28-Gbaud 16-QAM signal transmission through 40-km of standard SMF. Being low complexity/cost, the proposed transceivers can be considered as a promising candidate for future high-speed optical access networks.

Appendix

Derivation for Update Equation of c

The average of the error functions e_o and e_e are used to update c according to gradient decent algorithm as [26]:

$$c \leftarrow c - \mu_c \frac{\partial}{\partial c^*} \left\{ e_o e_o^* + e_e e_e^* \right\}$$

Now,

$$\begin{aligned} \frac{\partial}{\partial c^*} \left\{ e_o e_o^* \right\} &= e_o \frac{\partial e_o^*}{\partial c^*} + e_o^* \frac{\partial e_o}{\partial c^*} \\ &= e_o \frac{\partial}{\partial c^*} \left\{ d_o - x_o p_{11} c - x_e^* p_{12} c^* \right\}^* + e_o^* \frac{\partial}{\partial c^*} \left\{ d_o - x_o p_{11} c - x_e^* p_{12} c^* \right\} \end{aligned}$$

Noting that for a complex variable c, $\frac{\partial c}{\partial c^*} = 0$ and $\frac{\partial c^*}{\partial c^*} = 1$ and thus we get,

$$\frac{\partial}{\partial c^*} \left\{ e_o e_o^* \right\} = -e_o x_o^* p_{11}^* - e_o^* x_e^* p_{12}$$

Similarly,

$$\frac{\partial}{\partial c^*} \left\{ e_e e_e^* \right\} = -e_e x_o^* p_{21}^* - e_e^* x_e^* p_{22}$$

Therefore, the update equation for c is given as:

$$c \leftarrow c + \mu_c \left[e_o x_o^* p_{11}^* + e_o^* x_e^* p_{12} + e_e x_o^* p_{21}^* + e_e^* x_e^* p_{22} \right]$$

Derivation for Update Equation of h

The average of the error functions e_{ij} ($ij = 11$, 12, 21 and 22) are used to update the tap-coefficients of $\mathbf{h}$ according to least-square method as:

$$\mathbf{h} \leftarrow \mathbf{h} - \mu_h \frac{\partial}{\partial \mathbf{h}^*} \left\{ e_{11} e_{11}^* + e_{12} e_{12}^* + e_{21} e_{21}^* + e_{22} e_{22}^* \right\}$$

Now,

$$\frac{\partial}{\partial \mathbf{h}^*}\left\{e_{11}e_{11}^*\right\} = e_{11}\frac{\partial e_{11}^*}{\partial \mathbf{h}^*} + e_{11}^*\frac{\partial e_{11}}{\partial \mathbf{h}^*}$$
$$= e_{11}\frac{\partial}{\partial \mathbf{h}^*}\left\{d_o^*\{c^*/|c|\}^{-1} - \mathbf{h}^{*^T}\mathbf{x}^*(n-1)p_{11}^*\right\} + e_{11}^*\frac{\partial}{\partial \mathbf{h}^*}\left\{d_o\{c/|c|\}^{-1} - \mathbf{h}^T\mathbf{x}(n-1)p_{11}\right\}$$

For the vector $\mathbf{h}$, if we define $\frac{\partial}{\partial \mathbf{h}} = \left(\frac{\partial}{\partial h_0}, \frac{\partial}{\partial h_1}, \cdots, \frac{\partial}{\partial h_{N-1}}\right)^T$, it follows $\frac{\partial \mathbf{h}^{*^T}}{\partial \mathbf{h}^*} = \mathbf{I}$ and $\frac{\partial \mathbf{h}^T}{\partial \mathbf{h}^*} = \mathbf{O}$, where $\mathbf{I}$ and $\mathbf{O}$ are $N \times N$ identity and null matrices, respectively [26]. Therefore,

$$\frac{\partial}{\partial \mathbf{h}^*}\left\{e_{11}e_{11}^*\right\} = -e_{11}\mathbf{I}\mathbf{x}^*(n-1)p_{11}^* - e_{11}^*\mathbf{O}\mathbf{x}(n-1)p_{11}$$
$$= -e_{11}\mathbf{x}^*(n-1)p_{11}^*$$

Also,

$$\frac{\partial}{\partial \mathbf{h}^*}\left\{e_{12}e_{12}^*\right\} = e_{12}\frac{\partial e_{12}^*}{\partial \mathbf{h}^*} + e_{12}^*\frac{\partial e_{12}}{\partial \mathbf{h}^*}$$
$$= e_{12}\frac{\partial}{\partial \mathbf{h}^*}\left\{d_o^*\{c/|c|\}^{-1} - \mathbf{h}^T\mathbf{x}(n)p_{12}^*\right\} + e_{12}^*\frac{\partial}{\partial \mathbf{h}^*}\left\{d_o\{c^*/|c|\}^{-1} - \mathbf{h}^{*^T}\mathbf{x}^*(n)p_{12}\right\}$$
$$= -e_{12}\mathbf{O}\mathbf{x}(n)p_{12}^* - e_{12}^*\mathbf{I}\mathbf{x}^*(n)p_{12}$$
$$= -e_{12}^*\mathbf{x}^*(n)p_{12}$$

Similarly,

$$\frac{\partial}{\partial \mathbf{h}}\left\{e_{21}e_{21}^*\right\} = -e_{21}\mathbf{x}^*(n-1)p_{21}^*$$
$$\frac{\partial}{\partial \mathbf{h}}\left\{e_{22}e_{22}^*\right\} = -e_{22}^*\mathbf{x}^*(n)p_{22}$$

Putting all the terms together, we get,

$$\mathbf{h} \leftarrow \mathbf{h} + \mu_h\left\{e_{11}\mathbf{x}^*(n-1)p_{11}^* + e_{12}^*\mathbf{x}^*(n)p_{12} + e_{21}\mathbf{x}^*(n-1)p_{21}^* + e_{22}^*\mathbf{x}^*(n)p_{22}\right\}$$

References

[1] "IEEE P802.3ca 100G-EPON Task Force." 2015. [Online]. Available: http://www.ieee802.org/3/ca/index.html
[2] V. Houtsma, D. van Veen, and E. Harstead, "Recent progress on standardization of next generation 25, 50 and 100G EPON," *J. Lightw. Technol.*, vol. 35, no. 6, pp. 1228–1234, Mar. 2017.
[3] T. Minghui, L. Zhou, T. Zeng, T. Li, and X. Liu, "50-Gb/s/λ TDM-PON based on 10G DML and 10G APD supporting PR10 link loss budget after 20-km downstream transmission in the O-band," in *Proc. Opt. Fiber Commun. Conf.*, 2017, Paper Tu3G.2.
[4] T. Kodama, R. Matsumoto, and N. Suzuki, "Demonstration of data-rate and power-budget adaptive 100 Gb/s/λ-based coherent PON downlink transmission," in *Proc. Opt. Fiber Commun. Conf.*, 2017, Paper Th2A.22.
[5] E. Yamazaki *et al.*, "Fast optical channel recovery in field demonstration of 100-Gbit/s ethernet over OTN using real-time DSP," *Opt. Exp.*, vol. 19, no. 14, pp. 13179–13184, 2011.
[6] S. J. Savory, "Digital coherent optical receivers: Algorithms and subsystems," *IEEE J. Sel. Topics Quantum Electron.*, vol. 16, no. 5, pp. 1164–1179, Sep./Oct. 2010.
[7] K. Kikuchi, "Fundamentals of coherent optical fiber communications," *J. Lightw. Technol.*, vol. 34, no. 1, pp. 157–179, Jan. 2016.
[8] E. Ciaramella, "Polarization-independent receivers for low-cost coherent OOK systems," *IEEE Photon. Technol. Lett.*, vol. 26, no. 6, pp. 548–551, Mar. 2014.
[9] M. S. Erkılınç *et al.*, "Polarization-insensitive single-balanced photodiode coherent receiver for long-reach WDM-PONs," *J. Lightw. Technol.*, vol. 34, no. 8, pp. 2034–2041, Apr. 2016.
[10] S. Narikawa, H. Sanjoh, and N. Sakurai, "Coherent WDM-PON using heterodyne detection with transmitter-side polarization diversity," *IEICE Electron. Exp.*, vol. 7, no. 16, pp. 1195–1200, 2010.
[11] M. S. Faruk, H. Louchet, and S. J. Savory, "Robust single polarization coherent transceiver using DGD pre-distortion for optical access networks," in *Proc. Asia Commun. Photon. Conf.*, 2016, Paper AF1C–2.
[12] M. Rannello, M. Artiglia, M. Presi, and E. Ciaramella, "10 Gb/s long-reach PON system based on directly modulated transmitters and simple polarization independent coherent receiver," *Opt. Exp.*, vol. 25, no. 15, pp. 17841–17846, 2017.

[13] M. S. Faruk, H. Louchet, M. S. Erkılınç, and S. J. Savory, "DSP algorithms for recovering single-carrier Alamouti coded signals for PON applications," *Opt. Exp.*, vol. 24, no. 21, pp. 24083–24091, 2016.
[14] S. M. Alamouti, "A simple transmit diversity technique for wireless communications," *IEEE J. Sel. Areas Commun.*, vol. 16, no. 8, pp. 1451–1458, Oct. 1998.
[15] Y. Ja, "Analysis of four-port optical fiber ring and loop resonators using a 3 × 3 fiber coupler and degenerate two-wave mixing," *IEEE J. Quantum Electron.*, vol. 28, no. 12, pp. 2749–2757, Dec. 1992.
[16] C. Xie *et al.*, "Colorless coherent receiver using 3 × 3 coupler hybrids and single-ended detection," *Opt. Exp.*, vol. 20, no. 2, pp. 1164–1171, 2012.
[17] Y. Painchaud, M. Poulin, M. Morin, and M. Têtu, "Performance of balanced detection in a coherent receiver," *Opt. Exp.*, vol. 17, no. 5, pp. 3659–3672, 2009.
[18] R. Epworth, J. Whiteaway, and S. J. Savory, "3 fibre I and Q coupler," US Patent 6 859 586, Feb. 22, 2005.
[19] P. Anslow, C. Fludger, S. Savory, I. Hardcastle, and J. Fells, "Frequency selective coherent receiver for agile networks," in *Proc. Eur. Conf. Opt. Commun.*, 2006, pp. 1–2.
[20] K. Kikuchi and S. Tsukamoto, "Evaluation of sensitivity of the digital coherent receiver," *J. Lightw. Technol.*, vol. 26, no. 13, pp. 1817–1822, Jul. 2008.
[21] Y. Mori, C. Zhang, and K. Kikuchi, "Novel configuration of finite-impulse-response filters tolerant to carrier-phase fluctuations in digital coherent optical receivers for higher-order quadrature amplitude modulation signals," *Opt. Exp.*, vol. 20, no. 24, pp. 26236–26251, 2012.
[22] B. Zhang, C. Malouin, and T. J. Schmidt, "Design of coherent receiver optical front end for unamplified applications," *Opt. Exp.*, vol. 20, no. 3, pp. 3225–3234, 2012.
[23] T. Nakagawa *et al.*, "Non-data-aided wide-range frequency offset estimator for QAM optical coherent receivers," in *Proc. Opt. Fiber Commun. Conf.*, 2011, Paper OMJ1.
[24] D. Lavery, B. C. Thomsen, P. Bayvel, and S. J. Savory, "Reduced complexity equalization for coherent long-reach passive optical networks," *J. Opt. Commun. Netw*, vol. 7, no. 1, pp. A16–A27, 2015.
[25] I. Fatadin, S. J. Savory, and D. Ives, "Compensation of quadrature imbalance in an optical QPSK coherent receiver," *IEEE Photon. Technol. Lett.*, vol. 20, no. 20, pp. 1733–1735, Oct. 2008.
[26] S. Savory, "Digital equalization in coherent optical transmission systems," in *Enabling Technologies for High Spectral-Efficiency Coherent Optical Communication Networks*. Hoboken, NJ, USA: Wiley, 2016.